Research Article | Vol. 25, No. 2 | 23 Jan 2017 | OPTICS EXPRESS 1221

Optics EXPRESS

Tunable-focus lens for adaptive eyeglasses

NAZMUL HASAN,* AISHWARYADEV BANERJEE, HANSEUP KIM, AND CARLOS H. MASTRANGELO

Department of Electrical and Computer Engineering, University of Utah, Salt Lake City, Utah 84112, USA

nazmul.hasan@utah.edu

Abstract: We demonstrate the implementation of a compact tunable-focus liquid lens suitable for adaptive eyeglass application. The lens has an aperture diameter of 32 mm, optical power range of 5.6 diopter, and electrical power consumption less than 20 mW. The lens inclusive of its piezoelectric actuation mechanism is 8.4 mm thick and weighs 14.4 gm. The measured lens RMS wavefront aberration error was between 0.73 µm and 0.956 µm.

OCIS codes: (220.1080) Active or adaptive optics; (220.3620) Lens system design.

References and links

1. W. Tasman and E. A. Jaeger, *Duane's Ophthalmology* (LLW, 2013).
2. M. P. Keating, *Geometric, Physical and Visual Optics* (Butterworth-Heinemann, 2002).
3. S. H. Schwartz, *Geometrical and Visual Optics* (McGraw-Hill, 2002).
4. D. A. Goss and R. W. West, *Introduction to the Optics of the Eye* (Butterworth- Heinemann, 2001).
5. S. Resnikoff, D. Pascolini, S. P. Mariotti, and G. P. Pokharel, "Global magnitude of visual impairment caused by uncorrected refractive errors in 2004," Bull. World Health Organ. **86**(1), 63–70 (2008).
6. C. E. Letocha, "The invention and early manufacture of bifocals," Surv. Ophthalmol. **35**(3), 226–235 (1990).
7. L. Johnson, J. G. Buckley, A. J. Scally, and D. B. Elliott, "Multifocal spectacles increase variability in toe clearance and risk of tripping in the elderly," Invest. Ophthalmol. Vis. Sci. **48**(4), 1466–1471 (2007).
8. S. R. Lord, J. Dayhew, and A. Howland, "Multifocal glasses impair edge-contrast sensitivity and depth perception and increase the risk of falls in older people," J. Am. Geriatr. Soc. **50**(11), 1760–1766 (2002).
9. T. Callina and T. P. Reynolds, "Traditional methods for the treatment of presbyopia: spectacles, contact lenses, bifocal contact lenses," Ophthalmol. Clin. North Am. **19**(1), 25–33 (2006).
10. H. Ren and S.-T. Wu, *Introduction to Adaptive Lenses* (Wiley, 2012).
11. H. Jiang and X. Zeng, *Microlenses: Properties, Fabrication and Liquid Lenses* (CRC Press, 2013).
12. L. Alvarez, "Two-element variable power spherical lens," U.S. Patent Application 3305294 (1967).
13. L. W. Alvarez, "Development of variable- focus lenses and a new refractor," J. Am. Optom. Assoc. **49**(1), 24–29 (1978).
14. O. Aves, "Improvements in and relating to multifocal lenses and the like, and the method of grinding same," GB patent no. 15735 (1908).
15. C.-P. Chiu, T.-J. Chiang, J.-K. Chen, F.-C. Chang, F.-H. Ko, C.-W. Chu, S.-W. Kuo, and S.-K. Fan, "Liquid lenses and driving mechanisms: A review," J. Adhes. Sci. Technol. **26**(12), 1773–1788 (2012).
16. H. Ren, D. Fox, P. A. Anderson, B. Wu, and S.-T. Wu, "Tunable-focus liquid lens controlled using a servo motor," Opt. Express **14**(18), 8031–8036 (2006).
17. F. Carpi, G. Frediani, S. Turco, and D. De Rossi, "Bioinspired tunable lens with muscle-like electroactive elastomers," Adv. Funct. Mater. **21**(21), 4152–4158 (2011).
18. S. Shian, R. M. Diebold, and D. R. Clarke, "Tunable lenses using transparent dielectric elastomer actuators," Opt. Express **21**(7), 8669–8676 (2013).
19. M. Niklaus, S. Rosset, and H. Shea, "Array of lenses with individually tunable focal-length based on transparent ion implanted EAPs," Proc. SPIE **7642**, 76422K (2010).
20. N. Hasan, H. Kim, and C. H. Mastrangelo, "Large aperture tunable-focus liquid lens using shape memory alloy spring," Opt. Express **24**(12), 13334–13342 (2016).
21. H. Ren and S.-T. Wu, "Variable-focus liquid lens by changing aperture," Appl. Phys. Lett. **86**(21), 211107 (2005).
22. N. Peyghambarian, G. Li, and P. Ayras, "Adaptive electro-active lens with variable focal length," U.S. patent application 0164593 (2006).
23. C. W. Fowler and E. S. Pateras, "Liquid crystal lens review," Ophthalmic Physiol. Opt. **10**(2), 186–194 (1990).
24. A. Naumov, G. Love, M. Yu. Loktev, and F. Vladimirov, "Control optimization of spherical modal liquid crystal lenses," Opt. Express **4**(9), 344–352 (1999).
25. H. Ren, D. W. Fox, B. Wu, and S.-T. Wu, "Liquid crystal lens with large focal length tunability and low operating voltage," Opt. Express **15**(18), 11328–11335 (2007).
26. S. Sato, "Applications of liquid crystals to variable-focusing lenses," Opt. Rev. **6**(6), 471–485 (1999).

#280750 http://dx.doi.org/10.1364/OE.25.001221
Journal © 2017 Received 15 Nov 2016; revised 19 Dec 2016; accepted 24 Dec 2016; published 17 Jan 2017

Optics EXPRESS

27. G. Li, D. L. Mathine, P. Valley, P. Ayräs, J. N. Haddock, M. S. Giridhar, G. Williby, J. Schwiegerling, G. R. Meredith, B. Kippelen, S. Honkanen, and N. Peyghambarian, "Switchable electro-optic diffractive lens with high efficiency for ophthalmic applications," Proc. Natl. Acad. Sci. U.S.A. **103**(16), 6100–6104 (2006).
28. Fresnel Technologies Inc, "Fresnel lenses brochure," (2003) http:// www.fresneltech.com/pdf/FresnelLenses.pdf
29. H. Ren, Y. Fan, and S.-T. Wu, "Tunable Fresnel lens using nanoscale polymer-dispersed liquid crystals," Appl. Phys. Lett. **83**(8), 1515–1517 (2003).
30. S. Sato, A. Sugiyama, and R. Sato, "Variable-focus liquid-crystal fresnel lens," Jpn. J. Appl. Phys. **24**(8), 626–628 (1985).
31. Edmund Optics, "Fresnel lenses," http://www.edmundoptics.com/optics/optical-lenses/fresnel-lenses/2040/
32. L. Wang, H. Oku, and M. Ishikawa, "Variable-focus lens with 30 mm optical aperture based on liquid–membrane–liquid structure," Appl. Phys. Lett. **102**(13), 131111 (2013).
33. E. H. Mansfield, *The Bending and Stretching of Plates* (Cambridge University, 1989).
34. D. Armani, C. Liu, and N. Aluru, "Re-configurable fluid circuits by PDMS elastomer micromachining," in *Proceedings of Twelfth IEEE Conference on MEMS* (IEEE, 1999).
35. Q. Yang, P. Kobrin, C. Seabury, S. Narayanaswamy, and W. Christian, "Mechanical modeling of fluid-driven polymer lenses," Appl. Opt. **47**(20), 3658–3668 (2008).
36. N. Sugiura and S. Morita, "Variable-focus liquid-filled optical lens," Appl. Opt. **32**(22), 4181–4186 (1993).
37. F. Schneider, J. Draheim, R. Kamberger, P. Waibel, and U. Wallrabe, "Optical characterization of adaptive fluidic silicone-membrane lenses," Opt. Express **17**(14), 11813–11821 (2009).
38. M. S. Weinberg, "Working equations for piezoelectric actuators and sensors," J. Microelectromech. Syst. **8**(4), 529–533 (1999).
39. S. Pal and H. Xie, "Analysis and simulation of curved bimorph microactuators," Proc. NSTI-Nanotech **2**, 685–688 (2010).
40. S. A. Rios and A. J. Fleming, "A new electrical configuration for improving the range of piezoelectric bimorph benders," Sens. Actuators A Phys. **224**, 106–110 (2015).
41. Y. Wang, J. Balowski, C. Phillips, R. Phillips, C. E. Sims, and N. L. Allbritton, "Benchtop micromolding of polystyrene by soft lithography," Lab Chip **11**(18), 3089–3097 (2011).
42. D. R. Neal, R. J. Copland, D. A. Neal, D. M. Topa, and P. Riera, "Measurement of lens focal length using multicurvature analysis of Shack-Hartmann wavefront data," Proc. SPIE **5523**, 243–255 (2004).
43. C. Li, G. Hall, X. Zeng, D. Zhu, K. Eliceiri, and H. Jiang, "Three-dimensional surface profiling and optical characterization of liquid microlens using a Shack-Hartmann wave front sensor," Appl. Phys. Lett. **98**(17), 171104 (2011).
44. J. Porter, A. Guirao, I. G. Cox, and D. R. Williams, "Monochromatic aberrations of the human eye in a large population," J. Opt. Soc. Am. A **18**(8), 1793–1803 (2001).

1. Introduction

Degradation of vision is common in all human beings. The biological lens in our eyes starts to degrade creating refractive errors of vision by the age of 45. The four most common refractive errors of vision are myopia (nearsightedness); hyperopia (farsightedness), where far and nearby objects are seen out of focus, respectively; astigmatism, where vision is distorted by an irregularly curved cornea; and presbyopia which leads to loss of focal accommodation and difficulty in reading at arm's length [1–3]. Presbyopia is mostly an age related condition as the average accommodation range drops from 11 diopters on 20 year olds to 2 diopters by the age of 50 [4]. Worldwide in 2005, over one billion people were estimated to suffer from presbyopia alone [5].

Refractive errors cannot be prevented, but they are treated with corrective devices such as glasses, contact lenses, and refractive surgery. Eyeglasses correct refractive errors by shifting the focal plane by a fixed diopter amount, but often these tools do not provide satisfactory solutions. For example, many myopia and hyperopia sufferers often suffer from presbyopia as well; thus they may require several sets of eyeglasses with different mono-focal, bifocal, trifocal, and progressive lenses [6–9]. Eyeglasses cannot restore the accommodation range of a normal eye; hence these solutions partition the visible field onto smaller focal zones suitable to observe objects at different distances. Lens zoning greatly reduce the effective field of view; thus resulting in significant visual impairment.

The full field of view can be restored if the eyeglass lenses have a variable power that adaptively accommodates to the object distance. In order to address the need of most eyeglass corrected problems, the lens should have an accommodation range from –4 to + 4 diopters. Furthermore, the lenses should be light and thin with the aperture of 30-45 mm in diameter. The lens power should be adjusted at a minimum electrical power expense to ensure long

Optics EXPRESS

battery operation. In this paper we present the implementation of an electrically actuated variable power lens with aperture and power range suitable for adaptive eyeglass applications.

2. Variable focus lens technologies

Variable focus lenses (VFLs) change the curvature of the light wavefront in response to a control signal [10,11]. VFLs have been implemented using a variety of technologies, including sliding variable power rigid lenses [12–14], shape changing fluidic lenses [10,15–21], and voltage-controlled graded index (GRIN) liquid crystals (LCs) [10,22–27]. Each of these has its own unique set of virtues and limitations. Sliding-power lenses, for example, are very simple in construction but are subjected to friction and wear. They produce visible air gaps and very narrow field of views as well. Graded index (GRIN) LC lenses are attractive because they require very little electrical power. LC lenses works very well at small apertures (a few mm in diameter) but GRIN LCs cannot provide the phase changes needed for larger aperture lenses with the notable exception of "collapsed" grooved Fresnel configurations [28–30]. Fresnel configurations generally have image quality issues related to the visibility of the grooves and circular noise due to diffraction [28,29,31].

VFLs with larger apertures have also been realized with fluidic, flexible lenses by changing shape of peripheral rim, inserting liquid in or out, and by changing aperture [10,15–21]. A liquid lens usually consists of a cylindrical bladder with flexible front or back surfaces filled with a transparent optical fluid. The shape of the lens is changed by either pumping fluid in and out or by squeezing of the bladder. A major challenge in liquid VFLs is the selection of the actuation mechanism. Several approaches have been reported with various degrees of successes including electrical motors, electrostatic forces, electrophoretic motion, and more recently piezoelectric actuators [10,15]. The largest aperture electrically controlled variable-focus liquid lens is manufactured by Optotune with a clear aperture of 10 mm which is too small for eyeglass applications. Liquid VFL systems with larger apertures (~30 mm) have been recently demonstrated under table top laboratory conditions, but they have not been yet realized for light weight applications [32].

3. Variable focus eyeglasses

In this paper we demonstrate the realization of a liquid lens for eyeglass applications. The key features are its compact low weight and low profile design. Figure 1 shows a schematic cross-section of our lens without the actuators. The lens consists of a rigid annular sealing rim of gap, g_r encapsulated by two membranes forming a sealed chamber. This chamber is filled with a fixed volume of a high index optical fluid (glycerol n = 1.47). The top membrane has uniform thickness, t_t and radius, r_t. The bottom membrane has a rigid flat central piston of radius, r_p supported by a flexible annular membrane of thickness, t_b and radius, r_b. The thickness of the bottom membrane is made very thin such that the force required to flex it is negligible compared to that required to deform the top membrane. When a normal force, F_{piston} is applied to the bottom piston, the shape of the top membrane is changed. It bulges out or in depending on the direction of the force. This action thus produces a plano-convex or a plano-concave lens. The radius of the entire device is defined by the outer support rim and the lens thickness is defined by the piston displacement required for a given optical power change. The deflection requirement depends on the shape of the top membrane.

The top membrane deflection, u_o for a circular membrane of constant thickness under radial tension, T and uniform pressure, q_o satisfies the modified biharmonic Eq. (33),

$$D.\nabla^4 u_o - T.\nabla^2 u_o = q_o. \tag{1}$$

Here, D is the flexural rigidity of the membrane. The Eqs. for D and T are,

Optics EXPRESS

$$D = \frac{E \cdot t_t^3}{12(1-\mu^2)}, \qquad T = \varepsilon_i \cdot E \cdot t_t, \tag{2}$$

where ε_i is the initial membrane stretch, E is the membrane Young's modulus, and μ is the membrane Poisson's ratio.

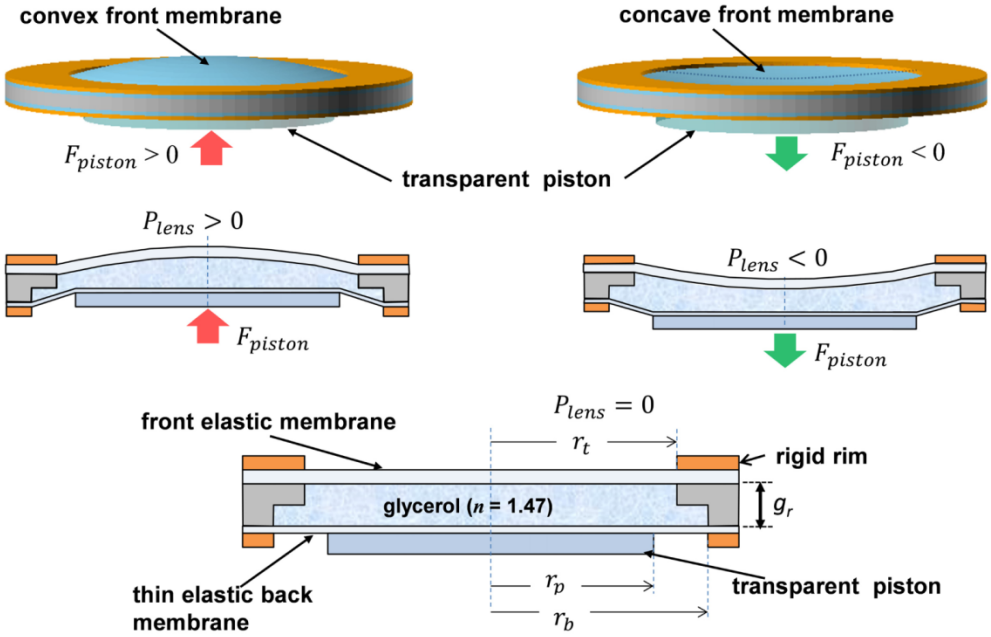

Fig. 1. Simplified schematic of soft membrane liquid lens excluding actuators. The lens optical power, P_{opt} is adjusted by vertically displacing the fluid, deflecting the top membrane thus changing its curvature.

The solution of Eq. (1) for any T and D for a circular diaphragm with clamped edge boundary condition is well known [33],

$$u_o = \frac{q_o \cdot r_t^2}{4 \cdot T}\left((1-\rho^2) + \frac{2}{\beta \cdot I_1(\beta)}(I_0(\beta\rho) - I_0(\beta))\right), \tag{3}$$

where $I_0()$ and $I_1()$ are the zero and first order modified Bessel functions of the first kind, $\beta = r_t \cdot \sqrt{\frac{T}{D}}$ is the normalized ratio of tension over rigidity, and $\rho = \frac{r}{r_t}$ is the normalized diaphragm radius. This solution has two well-known limits for tension and rigidity dominated regimes. The maximum deflection height, h at the membrane center ($r = 0$) is

$$h = u_o(0) = \frac{q_o \cdot r_t^2}{4.T}\left(1 + \frac{2(1-I_0(\beta))}{\beta}\right). \tag{4}$$

Note that, if tension is very large ($\beta >> 1$), Eq. (4) converges to, $h = \frac{q_o \cdot r_t^2}{4 \cdot T}$. In order to form a liquid lens, a spherical surface of radius of curvature, R is desired. Although the deformed membrane is not fully spherical, we approximate the deflection as a quadratic in ρ

Optics EXPRESS

corresponding to a spherical cap of radius R and maximum height h as shown in Fig. 2 satisfying the relationship,

$$(R-h)^2 + r_t^2 = R^2. \tag{5}$$

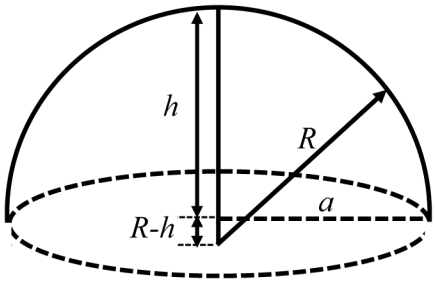

Fig. 2. A circular diaphragm under uniform tension, T and pressure, q_o forms approximately a spherical cap.

For typical lenses used for eyewear $h << r_t$; hence $R \approx r_t^2 / 2h$. Thus the lens optical power is,

$$P_{opt}(q_o) = \frac{(n-1)}{R} \approx \frac{2h(n-1)}{r_t^2} = \frac{q_o}{2 \cdot T}(n-1)\left(1 + \frac{2(1-I_0(\beta))}{\beta I_1(\beta)}\right). \tag{6}$$

The lens power is thus proportional to the pressure q_o. The top membrane displaced volume is the volume of the spherical cap,

$$\Delta V_{front}(q_o) = \frac{1}{6}\pi h(3r_t^2 + h^2) \approx \frac{1}{2} \cdot \pi \cdot h \cdot r_t^2. \tag{7}$$

Since the chamber volume is fixed the same liquid volume is displaced by the back membrane. If the back membrane is thin, narrow, and of negligible rigidity

$$\Delta V_{back}(q_o) \approx \frac{1}{2}\pi d_p (r_b^2 + r_p^2) = \Delta V_{front}(q_o) \approx \frac{1}{2}\pi h r_t^2 \Rightarrow h \approx \frac{(r_b^2 + r_p^2)}{r_t^2} d_p, \tag{8}$$

where d_p is the piston displacement. The piston force is, $F_{piston} = \pi r_b^2 q_o$. Combining Eq. (6) and (8), one obtains expressions for the piston spring constant k_p

$$k_p = \frac{F}{d_p} \approx 4\pi T \cdot \frac{r_b^2 (r_b^2 + r_p^2)}{r_t^4} \frac{1}{\left(1 + \frac{2(1-I_0(\beta))}{\beta I_1(\beta)}\right)}. \tag{9}$$

Equation (9) allows us to determine the piston displacement, d_p from the applied force. The optical power versus piston displacement is obtained from Eqs. (8) and (6),

$$P_{opt}(d_p) \approx 2(n-1)\frac{(r_b^2 + r_p^2)}{r_t^4} d_p. \tag{10}$$

At the default lens position, the two membranes are flat and the minimum rim gap is selected such that the membranes are not in contact for the largest piston displacement, or $(g_r)_{\min} \approx d_p$. This relationship defines the minimum volume and weight of liquid in the chamber as a function of the maximum lens power such that

Optics EXPRESS

$$V_{liquid} \geq \frac{\pi \cdot r_t^2 \cdot P_{\max}}{2(n-1)}. \tag{11}$$

Equations (9), (10), and (11) are useful to estimate some of the liquid lens parameters. For example, for an optical power change of + 3D with glycerol as the optical fluid and using top membrane radius of 18 mm, piston radius of 16 mm, and bottom membrane radius of 20 mm, the required piston displacement is 0.511 mm which is also the minimum gap. The minimum glycerin volume is thus ≈1.3 cm^3. For glycerin with density, ρ_o = 1.26 g/cc, this corresponds to a minimum liquid weight of 1.64 gr. In practice, the lens weight will also be affected by the thickness and weight of the frame.

The force required to move the piston depends on the initial tension parameter, *T*. The top and bottom membranes are made of polydimethylsiloxane (PDMS) with thicknesses of 1.2 mm and 0.2 mm, respectively. The Young modulus and tension of these membranes can vary significantly depending on the PDMS mixture formulation and curing cycle [34]. We measured these parameters using the deflection method described in Yang et al. [35]. The value of Young's modulus, Poisson's ratio, and pre-strain were 987.6 kPa, 0.49, and 2.83%, respectively. This pre-strain yields a pre-tension of 33.5 N/m. The calculated piston force required for the optical power change of + 3 D was 0.75N or 76 gm consistent with these parameters.

4. Control of hydrostatically induced coma aberrations

The front diaphragm deformation is not only subject to the piston force but also the effects of gravity. If the lens is standing upright on its edge, gravity produces hydrostatic pressure which increases linearly from the top to the bottom of the lens. This hydrostatic pressure adds to that of the piston thus producing a non-spherical deformation and asymmetric bulging of the diaphragm. This lens shape distortion produces a significant amount of coma aberration [36,37] that must be minimized for acceptable optical performance. The deformation of membranes under symmetric hydrostatic pressure is given in [32],

$$u_h = \frac{\rho_o g r_t^3 (1-\rho^2)\cos(\theta)}{8T}\left(1 - \frac{2(I_1(\beta) - I_2(\rho\beta))}{\beta(1-\rho^2)I_2(\beta)}\right). \tag{12}$$

Where *g* is the gravitational acceleration (9.8 m/s^2), θ is the angle respect to the vertical axes, and $I_2()$ is the second order modified Bessel functions of the first kind. The hydrostatic pressure produces an *S*-type deflection that adds to the symmetric deflection of Eq. (3). The net effect of the distortion is that the optical power at the top is lower than the bottom of the lens. The slope of the distorted lens power versus height *y* at the lens center can be calculated from the mean curvature of Eq. (12) as,

$$\left.\frac{\partial P_{opt}}{\partial y}\right|_{r=0} \approx -\frac{\rho_o g}{2T}(n-1)\left(1 - \frac{\beta^2}{8I_2(\beta)}\right). \tag{13}$$

The calculated and measured slopes of the optical power at the center of the lens are −0.084 D/mm and −0.09 D/mm respectively. The power uniformity and quality of the lens image however can be arbitrarily improved if the tension is increased at the expense of optical power range. Coma can be reduced further or nearly eliminated with liquid-membrane-liquid lenses [32]. These lens configurations rely on the utilization of liquids of equal densities but different index on both sides of deflecting membranes. The primary disadvantage of this coma elimination method is that optical power is severely reduced as it is proportional to the index difference between two similar liquids (~0.2) compared to much larger index differences between optical liquids and air (0.5-0.7).

Optics EXPRESS

5. Piston actuation mechanism

The central part of the lens (the bossed piston) is transparent and unobstructed; therefore the piston actuators are placed along the lens periphery as shown in Fig. 3. The piston moves up and down driven by three low-profile curved piezoelectric bimorph actuators. The points of contact of the three bimorphs with the piston thus define the backside plane of the liquid lens.

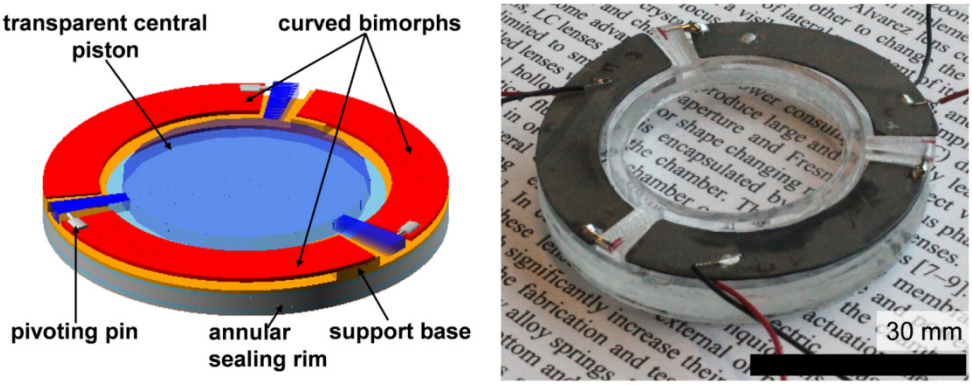

Fig. 3. Schematic of the bimorphs actuating the bossed membrane lens (left) and photo of the actual device (Right).

The vertical and angular deflections of curved bimorphs are [38,39]

$$U(R,s)=\frac{M_b\cdot R^2}{E_b\cdot I_b}\cdot(1-\cos(\frac{s}{R})),$$
$$\varphi(s)=\frac{U(s)}{R}, \tag{14}$$

where $U(s)$ is the vertical deflection at the mid radius R as a function of the length s along the bimorph mid radius, and $\varphi(s)$ is the bimorph tilt angle as shown in Fig. 4. The parameters E_b and I_b are the bimorph's Young's modulus and moment of inertia, respectively and M_b is the bimorph's piezoelectric moment,

$$M_b=w_b\cdot E_b\cdot d_{31}\cdot t_b\cdot V_b, \tag{15}$$

where w_b is the bimorph's beam width, t_b is the thickness of each bimorph layer, d_{31} is the bimorph's piezoelectric coefficient and V_b is the applied voltage across the bimorph actuator.

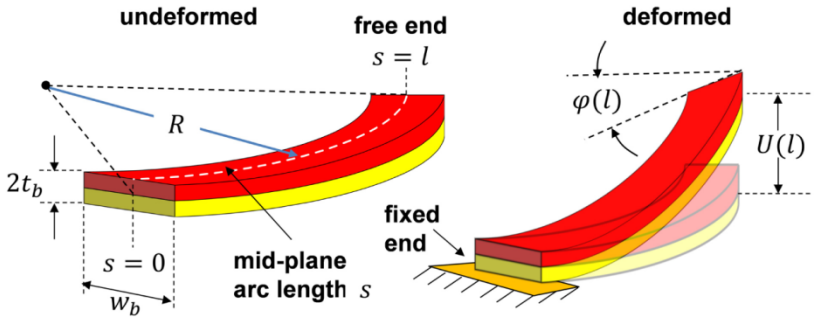

Fig. 4. Deflection of a curved bimorph. Since the outer edge is longer than the inner one, this type of actuator not only bends but also rotates at its tip.

Optics EXPRESS

For efficient deflection, the end support of the bimorph must pivot about the highest elevation point, the end of the bimorph outer radius. For example, a 22.5 mm radius actuator 5 mm wide and an angle of 115°, a 1 mm mid-radius deflection yields a rotation angle of 2.5° and a difference in deflection of 20% between the inner and outer radius. In order to get maximum deflection from the actuators without compromising the actuator force, we used a pinning-hole end configuration. Rigid pins are thus attached near the highest elevation point of the actuators (the outer farthest corner). The pins pivot inside cylindrical holes drilled inside three extension tabs connected to the central piston. The curved actuators were implemented using thin PZT 5H4E bimorphs with dimensions and characteristics shown in Table 1. Each bimorph actuator weighs less than 1 gm.

Table 1. Curved Bimorph Characteristics.

Bimorph Material	PZT 5H4E
Layer Thickness, t_b	270 μm
Width, w	8.2 mm
Young's Modulus, E	$5x10^{10}$ N/m^2
Piezoelectric Strain Coefficient, d_{31}	$-320x10^{-12}$ m/V
Radius of Curvature, R	21 mm
Angle of Cosine, (s/R)	110°-113°
Voltage Range	0-250 V

Combining Eqs. (10), (14), and (15), we can obtain an expression for the lens optical power as a function of actuator parameters, liquid refractive index, lens dimensions, and operating voltage. If we drive each lens with three bimorphs, one obtains the optical power

$$P_{opt} \approx \frac{2(n-1)\cdot U(R,s)\cdot (r_b^2 + r_p^2)}{r_t^4 \cdot (1+\frac{k_p}{3k_b})}. \qquad (16)$$

Where k_p is the piston spring constant of Eq. (9) and k_b is the vertical spring constant of one bimorph at the pinhole support. The bimorph spring constant was measured as k_b ~390 N/m. The optical power in Eq. (16) increases linearly with the actuator voltage V_b. As the membrane and piston are made stiffer, the spring constant of the bimorph actuator k_b itself becomes important, and the lens membrane deflection and observed optical power is gradually reduced.

6. High-voltage driver circuits

The bimorphs require multiple high voltage control signals. For evaluation purposes, a fixed 300V DC voltage source was used to power the driver circuits. The high voltage DC can also be generated using miniature 3V DC-to-DC converters (EMCO-A series) suitable for battery driven setups. The fixed DC voltage was converted to variable voltages using pulse width modulators (PWMs). Each PWM modulator was implemented using a high voltage half-bridge driver circuit (ST Micro L6384E), two high voltage NMOS transistors (ST Micro IRF820) and a high-voltage 100 nF capacitor. The pulsed half-bridge drivers were driven by a microcontroller through opto-isolators. The bimorphs were driven in a bipolar two-terminal series configuration using two unipolar PWM high-voltage circuits in differential drive configuration. A software open loop control system was implemented to control the bimorph deflection and the lens optical power. The bimorph bending magnitude and direction was changed by adjusting the duty cycle of the PWM signal and driving from only one of the opposing PWM drivers at any given time.

In addition to series bimorphs, other more efficient three-terminal configurations are also possible [40]. Y-poled (polling direction same) three-wire bimorphs were also tested for actuation in a bipolar configuration [40]. The bipolar configuration provides 30% more

Optics EXPRESS

deflection with higher actuation force but requires higher voltages. Lenses were made and tested with both configurations, but the series bimorph configuration was our preferred implementation due to its simplicity.

7. Fabrication

7.1 Lens frame and pistoned liquid chamber

The lens rim was constructed by cutting acrylic sheet with laser (VLS 3.60, Universal Laser Systems) with 100% power and 10% speed for through cut and with 20% speed for making notches. The lens rim height was 2.5 mm and the lens rim had a notch of 1 mm in one side. The inner and outer radius of the rim was 18 mm and 26 mm, respectively. The radius in the notched part of the rim, r_b was 20 mm. The front and back elastic membranes were made of polydimethylsiloxane (PDMS). The thicknesses of front and back membranes were 1.2 mm and 0.2 mm respectively. A PDMS silicone elastomer (Sylgard 184, Dow Corning) was used in 7.5:1 ratio of base and curing agent to fabricate the PDMS membranes at 60° C for 6 hours. After fabricating the membranes, the 0.2 mm thick back membrane was attached to the notched side of the rim and front membrane to the other side. Both membranes were attached to the acrylic rim using a thin layer of silicone sealing adhesive from Dow Corning (734 Flowable Sealant). A thin solid transparent piston was next attached to the back membrane with optically clear urethane rubber (Clear Flex). The urethane rubber mixture was spun for 550 rpm for 1 minute to get a uniform thin layer (<0.1 mm) and the piston was kept over the thin back membrane for 16 hours to let the adhesive set. The transparent piston was 4 mm thick and it has three extending arms with three pinning holes as shown in Fig. 3.

7.2 Lens chamber liquid filling

Two holes were drilled on the annular sealing rim for insertion of the optical lens fluid and venting of air. Glycerol is used as the liquid because it has both high refractive index (n = 1.47) and does not swell the PDMS membrane, but other higher index optical fluids (SantoLight5267, n = 1.67) are available as well [32,41]. For a liquid lens filled with glycerol with density of 1.26 g cm^{-3}, a lens with vertical height of 36 mm can produce a maximum hydrostatic pressure difference of $P_{hyd} = g \cdot \rho_g \cdot h$ = 444.5 Pa between inside and outside of the lens. Therefore, if glycerol is inserted into the chamber at atmospheric conditions, the front membrane bulges significantly outward, which makes the initial lens optical power high. The hydrostatic pressure drop deflection is significantly reduced if the lens reservoir is pressure equilibrated and hermetically sealed. Pressure equilibration is achieved when the lens cavity is filled in by bath immersion, in this case in a mixture of 3:2 glycerol and water, such that at any given point pressure inside and outside the lens are almost equal thus producing little deformation of the membranes during the fill operation. The two holes are next hermetically sealed while the lens is submerged. The lens is next pulled out of the glycerin bath, rinsed and dried. The hermetic seal produces a vacuum head pressure that counteracts fluid motion driven by gravity producing a much smaller lens deformation. After sealing of the lens chamber, a 0.5 mm thick acrylic washer was attached to the front side of the lens. A second 1 mm thick washer was attached to the back side with raised supports for the bimorphs.

7.3 Curved bimorphs

The pinned piston-actuator design configuration overcomes the twisting problem of the curved actuators and provides maximum vertical deflection without compromising force. We constructed curved bimorphs actuators from thin sheets of pre-poled PZT-4H (T223-H4CL-503X for two terminal actuators and T220-H4-503Y for three terminal actuators from Piezo System Inc.). The actuator sheet was cut into the curved shape using a diamond rotary saw followed by grinding and soldering of the end pin joint. Strong nickel plated steel pins were soldered to the outer most point of the free ends of the actuators. One end of each curved

Optics EXPRESS

actuator was glued to the actuator supports on the rim. The other pinned end of the actuator is a free moving end which was inserted in the piston tab receiving holes.

8. Results and discussion

8.1 Lens optical test setup

A Shack-Hartmann wavefront sensor (SHS) (WFS150-7AR from ThorLabs) and a collimated LED light source (M625L3-C1 from ThorLabs) with wavelength 625 nm were used for measuring lens optical power and wavefront aberration. The setup is also described in Hasan et al. [21]. All optical measurements were recorded with the lens standing in vertical position which is the worst case scenario for coma aberration. In order to measure the lens focal length as a function of applied voltage, we utilized the proximity technique [42]. In the proximity technique, the test lens was placed 1.4 cm apart from the wavefront sensor lenslet array in the vertical direction and the collimated light source was 50 cm apart from the test lens as shown in Fig. 5(a). As the incoming beam into the test lens is collimated, the lens focal length, $f_L = R$ (radius of curvature of incoming light) $-L$ (separation of test lens and sensor) [42].

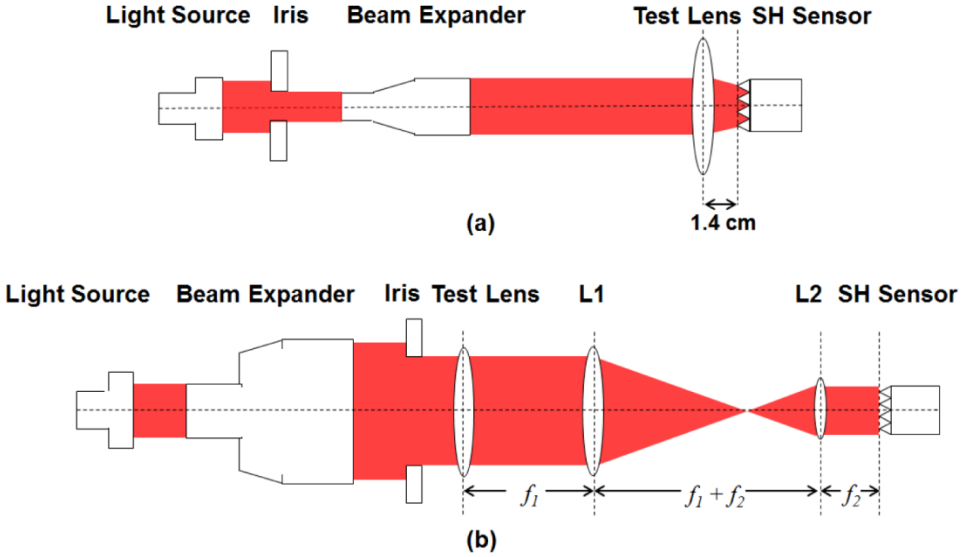

Fig. 5. (a) Proximity technique for lens focal length measurement and (b) 4*f* optical setup for lens aberration measurement.

For measuring the lens wavefront aberration, we profiled the central 25 mm diameter of the possible 32 mm aperture of the lens as discussed in [21,35]. As the diameter of the SHS sensor is small (~4.6 mm), the SHS sensor cannot profile the 25 mm diameter aperture of our test lens. For this, a *4f* afocal relay lens system was constructed that feeds all lens light into the sensor as shown in Fig. 5(b) [43]. When the test lens focal length is infinity, the afocal relay lens system reduces the incoming light beam diameter by ~5.7 fold. The Shack-Hartmann sensor was located f_2 away from the second relay lens and its pupil diameter was selected as 4.3 mm. The focal length of the test lens can also be measured by the relay lens system; however, the influence of the test lens focal length on the entire system is greatly reduced because of the beam reduction ($f_2/f_1 << 1$). Therefore, the proximity technique is preferred for focal length measurement and the *4f* relay system for measuring wavefront aberration. The relay lens setup has RMS wavefront aberration of 0.15 µm.

Optics EXPRESS

8.2 Optical power measurement

The lens operation is straightforward. If the voltage is applied and increased in positive direction, the three bimorph actuators along with the piston moves inward direction. It makes the front membrane convex. For negative actuator voltage, the piston moves outward making the lens concave. The proximity technique was used to measure the lens optical power at the center of the lens under various actuation voltages. Figure 6 shows the lens optical power as a function of actuator voltage.

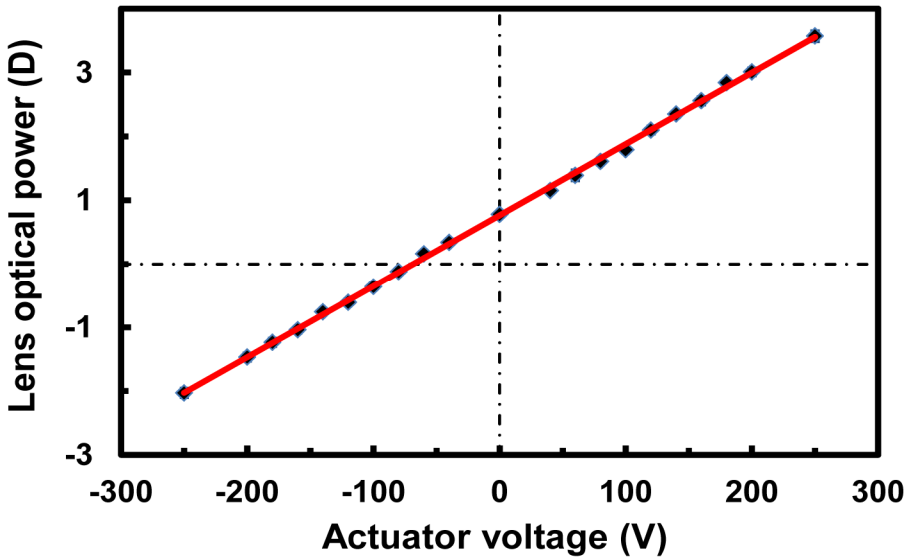

Fig. 6. Lens optical power (at the lens center) as a function of voltage. The standard deviations of lens power are below 1.3%.

The lens has an offset power of + 0.78D when unpowered. The lens optical power ranged between –2.03 D to + 3.57 D for a voltage range of –250 V to + 250 V, which was below the depolarization voltage for our bimorph actuators. The lens optical power is linearly proportional with the actuator voltage as expected. To demonstrate the quality of the lens image, the lens focal length was tuned continuously using the driver circuit and photos were taken at different lens power. The test lens was attached to a single lens reflex camera with 40

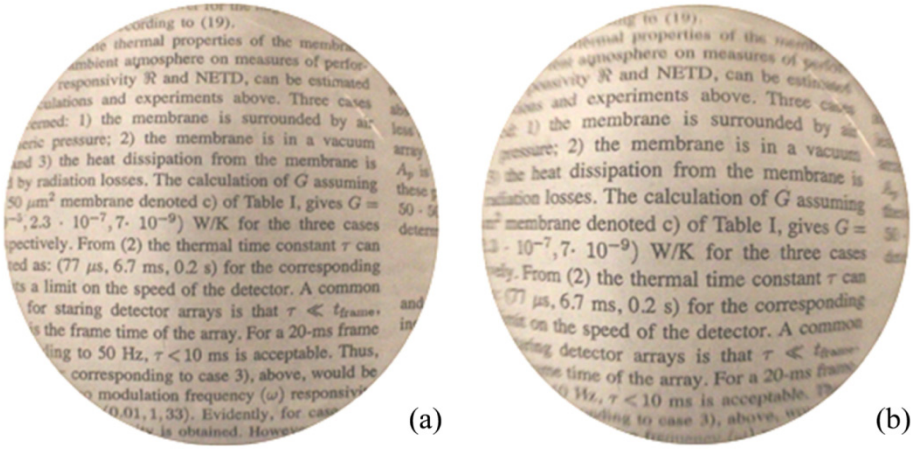

Fig. 7. Target object photos taken through the VFL lens at (a) –1.2 diopter (b) + 3 diopter.

Optics EXPRESS

mm focal length. The target object was placed 35 cm apart from the test lens. Figure 7 shows two photos taken through our fabricated lens at different lens power.

The lens electrical power consumption and its mechanical resonance were also measured as shown in Fig. 8. The electrical power dissipation for the lens was very small, in the range of 10-20 mW. This is good low power performance as these lenses can be operated from lightweight rechargeable portable batteries. With an 8 gm, 110 mAh LiPo battery and a DC-DC high voltage converter (EMCO A series), the lens can continuously operate for about 6 hours. One of the important advantages for piezoelectric bimorph actuators is the zero static power consumption; hence battery lifetime can be significantly extended if the focal change frequency is reduced.

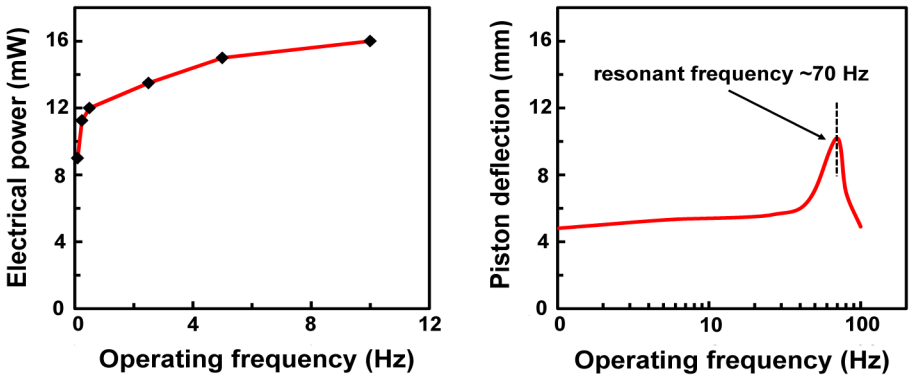

Fig. 8. (left) Lens electrical power consumption (at 160 V) as a function of switching frequency and (right) lens actuators' mechanical displacement as a function of frequency.

The mechanical resonance of the structure determines the speed of response for the lens. The frequency response of the lens was measured by observing the deflection of the lens piston (via a bouncing laser beam) projected onto a screen as a function of bimorph driving frequency. The lens displayed a resonant frequency of about 70 Hz which makes the effective response time about 15 milliseconds. The lens was operated continuously for more than 500 cycles with the driving circuit in the voltage range of –220 V to + 220 V without observing any failure or significant performance degradation as well. It was also actuated intermittently for more than 6 months without any failure.

9. Wavefront profiling and aberration measurements

To evaluate lens optical performance and image quality, the lens aberrations were measured with the lens in the upright position by the SHS using *4f* optical test setup (shown in Fig. 5(b)). The wavelength of the collimated test light source was 0.625 µm. The aberration values at no actuation (+ 0.78 D), lens convex, and concave states are reported in Table 2.

Table 2. Lens Aberrations at different optical power.

Aberration	Optical power + 0.78 D	Optical power + 3 D	Optical power –1 D
Astigmatism 45°	–0.364 µm	–0.354 µm	0.376 µm
Astigmatism 90°	–0.380 µm	0.343 µm	0.400 µm
Trefoil X	–0.008 µm	–0.035 µm	–0.056 µm
Trefoil Y	–0.007 µm	–0.385 µm	0.070 µm
Coma X	0.298 µm	–0.208 µm	–0.153 µm
Coma Y	–0.7400 µm	–0.264 µm	–0.608 µm
Spherical	–0.068 µm	–0.188 µm	–0.119 µm
RMS Aberration	0.958 µm	0.733 µm	0.846 µm

Optics EXPRESS

The main contributor for RMS wavefront aberration at + 0.78 D (no actuation) was coma. Coma aberration is proportional to the third power of the radius of the lens and inversely proportional to the membrane tension as shown in Eq. (12). Coma aberration was worst at no actuation and it decreased significantly at higher optical power. Spherical aberration was very small at no actuation, and it increased a little at high optical power. The low values of spherical aberration are indicative of the tension dominated membrane deflection [35]. The value of trefoil aberration also increased from negligible value to 0.385 μm as the lens optical power increased because the actuators applied forces at three different points 120° apart along the periphery. All these aberration values except coma were relatively small and below 0.5 μm which is the approximate RMS value of human lens aberration [44]. The 80% encircled energy radii of the point spread function (PSF) were measured at three different lens optical powers as well. The values were 0.1°, 0.065°, 0.065° at lens optical power + 0.78 D, + 3 D and −1D, respectively.

10. Conclusion

A tunable-focus liquid lens actuated by low-profile piezoelectric bimorph actuators has been demonstrated. The lens has aperture diameter 32 mm, footprint diameter 52 mm, optical power range 5.6 D, electrical power consumption less than 20 mW, and resonant frequency 70 Hz. The lens weighs 14.4 gm. The lens RMS wavefront aberration is in the range of 0.73 to 0.95 μm. All these criteria make this lens suitable for adaptive eyeglass application.

11. Funding

This project is sponsored by the US National Institute of Health NIBIB 1U01EB023048-01 cooperative agreement.